

Galaxy And Mass Assembly (GAMA): Resolving the role of environment in galaxy evolution

S. Brough^{1*}, S. Croom², R. Sharp³, A. M. Hopkins¹, E. N. Taylor^{2,4}, I. K. Baldry⁵,
 M. L. P. Gunawardhana^{2,1}, J. Liske⁶, P. Norberg⁷, A. S. G. Robotham^{8,9},
 A. E. Bauer¹, J. Bland-Hawthorn², M. Colless¹, C. Foster¹⁰, L. S. Kelvin^{9,8,11},
 M. A. Lara-Lopez¹, Á.R. López-Sánchez^{1,12}, J. Loveday¹³, M. Owers¹,
 K. A. Pimbblet¹⁴, M. Prescott¹⁵

¹ *Australian Astronomical Observatory, PO Box 915, North Ryde, NSW 1670, Australia*

² *Sydney Institute for Astronomy (SIFA), School of Physics, The University of Sydney, NSW 2006, Australia*

³ *Research School of Astronomy & Astrophysics, The Australian National University, Cotter Road, Weston Creek, ACT 2611, Australia*

⁴ *School of Physics, The University of Melbourne, Parkville, VIC 3010, Australia*

⁵ *Astrophysics Research Institute, Liverpool John Moores University, Twelve Quays House, Egerton Wharf, Birkenhead CH41 1LD, UK*

⁶ *European Southern Observatory, Karl-Schwarzschild-Str. 2, 85748 Garching, Germany*

⁷ *Institute for Computational Cosmology, Department of Physics, Durham University, South Road, Durham DH1 3LE, UK*

⁸ *ICRAR, University of Western Australia, 35 Stirling Highway, Crawley, WA 6009, Australia*

⁹ *SUPA, School of Physics and Astronomy, North Haugh, St Andrews, Fife, KY169SS, UK*

¹⁰ *European Southern Observatory, Alonso de Cordova 3107, Vitacura, Santiago, Chile*

¹¹ *Institut für Astro- und Teilchenphysik, Universität Innsbruck, Technikerstraße 25, 6020 Innsbruck, Austria*

¹² *Department of Physics and Astronomy, Macquarie University, NSW 2109, Australia*

¹³ *Astronomy Centre, University of Sussex, Falmer, Brighton BN1 9QH, UK*

¹⁴ *School of Physics, Monash University, Clayton, VIC 3800, Australia*

¹⁵ *Department of Physics, University of the Western Cape, Private Bag X17, Bellville 7535, South Africa*

ABSTRACT

We present observations of 18 galaxies from the Galaxy And Mass Assembly (GAMA) survey made with the SPIRAL optical integral field unit (IFU) on the Anglo-Australian Telescope. The galaxies are selected to have a narrow range in stellar mass ($6 \times 10^9 M_{\odot} < M_* < 2 \times 10^{10} M_{\odot}$) in order to focus on the effects of environment. Local galaxy environments are measured quantitatively using 5th nearest neighbour surface densities. We find that the total star formation rates (SFR) measured from the IFU data are consistent with total SFRs measured from aperture correcting either GAMA or Sloan Digital Sky Survey single-fibre observations. The mean differences are $\text{SFR}_{\text{GAMA}}/\text{SFR}_{\text{IFU}} = 1.26 \pm 0.23$, $\sigma = 0.90$ and for the Sloan Digital Sky Survey we similarly find $\text{SFR}_{\text{Brinchmann}}/\text{SFR}_{\text{IFU}} = 1.34 \pm 0.17$, $\sigma = 0.67$. Examining the relationships with environment, we find off-centre and clumpy H α emission is not significantly dependent on environment, being present in 2/7 (29_{-11}^{+20} per cent) galaxies in high-density environments ($> 0.77 \text{ Mpc}^{-2}$), and 5/11 (45_{-13}^{+15} per cent) galaxies in low-density environments ($< 0.77 \text{ Mpc}^{-2}$). We find a weak but not significant relationship of the total star formation rates of star-forming galaxies with environment. Due to the size of our sample and the scatter observed we do not draw a definitive conclusion about a possible SFR dependence on environment. Examining the spatial distribution of the H α emission, we find no evidence for a change in shape or amplitude of the radial profile of star-forming galaxies with environment. If these observations are borne out in larger samples this would infer that any environment-driven star-formation suppression must either act very rapidly (the ‘infall-and-quench’ model) or that galaxies must evolve in a density-dependent manner (an ‘in-situ evolution’ model).

Key words: galaxies: elliptical and lenticular, cD — galaxies: evolution — galaxies: kinematics and dynamics — galaxies: clusters: general

1 **1 INTRODUCTION**

2 The galaxy population we see today has some very distinctive
3 features. One of the most fundamental is the separation
4 of galaxies into a bimodal distribution according to colour
5 (e.g. Strateva et al. 2001; Baldry et al. 2006). The colour
6 largely relates to the age of the stars, with galaxies on the
7 tight red sequence being mostly passive systems containing
8 old stars. In contrast, the galaxies in the blue cloud generally
9 show a younger stellar population (e.g. Taylor et al. in prep).
10 However, it is still unclear what drives this separation.

11 Recent research has focussed on how blue star-forming
12 galaxies can have their star formation quenched, moving
13 them onto the red sequence. Red-sequence galaxies are prefer-
14 entially found in denser environments (e.g. Blanton et al.
15 2005; Cooper et al. 2008; Thomas et al. 2010; Smith et al.
16 2012) and star formation is also clearly suppressed in those
17 high density environments (e.g. Lewis et al. 2002; Gómez
18 et al. 2003; Kauffmann et al. 2004). This immediately sug-
19 gests environmental factors play an important role.

20 There is uncertainty, however, in how the change in star-
21 forming properties as a function of environment manifests
22 itself. Balogh et al. (2004) found that, once luminosity is
23 taken into account, the observed environmental difference is
24 only due to the *fraction* of blue galaxies changing in each
25 environment, rather than due to any change in the proper-
26 ties of the galaxy population. Star formation rates measured
27 from single-fibre observations of the H α emission line give
28 similar conclusions: Peng et al. (2010) observed that the re-
29 lationship between star formation rate and stellar mass was
30 the same in the highest and lowest density environments. Re-
31 cent results from the Galaxy And Mass Assembly (GAMA;
32 Driver et al. 2011) survey also show that the fraction of star-
33 forming galaxies falls with increasing environmental density
34 (Wijesinghe et al. 2012; Robotham et al. 2013), but the star
35 formation rate of the star-forming galaxies depends solely
36 on their stellar mass, showing no change with their envi-
37 ronment (Wijesinghe et al. 2012). These observations would
38 imply that any mechanism that transforms galaxies in dense
39 environments must be rapid or have happened a long time
40 ago.

41 In contrast, research examining the strength of the
42 4000Å break and the Balmer absorption lines (von der Lin-
43 den et al. 2010) and ultraviolet imaging from the *GALaxy*
44 *Evolution EXplorer* (GALEX) space telescope (Rasmussen
45 et al. 2012) suggests that both the star-forming fraction *and*
46 the star formation rate in star-forming galaxies changes as a
47 function of environment, allowing for a longer timescale for
48 any transformation.

49 The different conclusions drawn by these observations
50 may have a number of causes, including the different ways
51 that star formation and environment are measured, vary-
52 ing definition for star-forming galaxies and the inability of
53 single-fibre observations to specify where that star forma-
54 tion is happening. This last point is crucial given that the
55 proposed mechanisms for any modulation of star formation
56 with environment can have very different spatial effects:

57 *Ram-pressure stripping* (Gunn & Gott 1972; Nichols &
58 Bland-Hawthorn 2011), which can expel the gas from the
59 disk, and *strangulation* (Larson et al. 1980), which results
60 when the gas is removed from the halo, should both prefer-
61 entially remove gas in the outer parts of galaxies (e.g. Bekki

62 2009; Kapferer et al. 2009). These processes may be efficient
63 at removing halo gas, which is observed in galaxy clusters
64 (e.g. Sun et al. 2007; Randall et al. 2008). Ram-pressure
65 stripping may also act in small and/or compact groups (Mc-
66 Carthy et al. 2008; Rasmussen et al. 2008) or on the out-
67 skirts of clusters (e.g. Merluzzi et al. 2013). The timescale
68 of > 2 Gyrs for strangulation (McCarthy et al. 2008), how-
69 ever, seems to contradict the short timeframe implied by
70 observations. Although Prescott et al. (2011) find this to be
71 the likely mechanism for the quenching of star formation in
72 satellites hosted by isolated galaxies. Direct galaxy–galaxy
73 interactions may also play a critical role in either trigger-
74 ing star formation (e.g. Moss & Whittle 1993; Ellison et al.
75 2008; Patton et al. 2013) or suppressing it, as seen in the
76 less-massive galaxies of pairs when the pair mass ratio is
77 large (Robotham et al. 2013).

78 Feedback from star formation in low-mass galaxies pro-
79 vides an internal mechanism for transformation. This pro-
80 vides a solution to the mismatch of the theoretical dark mat-
81 ter halo mass function and the observed stellar mass function
82 (e.g. Baldry et al. 2008) by heating and/or expelling gas in
83 halos. Extreme outbursts of star formation may be triggered
84 by mergers or interactions (e.g. Hopkins et al. 2009) even
85 with very low luminosity galaxies or tidal debris (e.g. López-
86 Sánchez 2010; Cluver et al. 2013), and frequently seen in iso-
87 lated compact groups (e.g. López-Sánchez et al. 2004; Kon-
88 stantopoulos et al. 2010; Scudder et al. 2012). This makes
89 a link between internal and environmental effects. There is
90 observational evidence of feedback from star formation (e.g.
91 Veilleux et al. 2005; Strickland & Heckman 2009; López-
92 Sánchez et al. 2012).

93 At present it is still not clear which of these processes
94 dominate in which situations. In one of the first attempts to
95 study spatially-resolved star formation in a very large sam-
96 ple as a function of a broad range of environment, Welikala
97 et al. (2008, 2009) used galaxy colours to demonstrate that
98 star formation is suppressed in the central parts of galaxies
99 in high-density environments, apparently ruling out ram-
100 pressure stripping as a significant influence in the general
101 galaxy population.

102 While galaxy colours are a coarse measure of the
103 integrated star formation history of a galaxy, the well-
104 understood H α emission line at 6563Å probes near-
105 instantaneous star formation (< 10 Myr, e.g. Kennicutt
106 1998). Spatially-resolved H α measurements have only been
107 made for samples of local galaxies either in the field or
108 nearby clusters (e.g. Moss & Whittle 1993; Vogt et al. 2004;
109 Koopmann & Kenney 2004; Meurer et al. 2006; Fumagalli
110 & Gavazzi 2008; Rose et al. 2010; Sánchez et al. 2012), often
111 with narrow-band imaging, but have not been possible for a
112 data set that covers a wide range in environment.

113 We present here observations of the spatially-resolved
114 H α emission of galaxies over a wide range of environment
115 from optical integral field unit (IFU) observations of galax-
116 ies selected from the GAMA survey. The primary goal of
117 this paper is to measure the radial distribution of star forma-
118 tion and examine how that varies as a function of envi-
119 ronment. We know that the star formation rates of galax-
120 ies are strongly dependent on their stellar mass, but their
121 dependence on environment is less clear. We therefore use
122 GAMA to select a carefully controlled sample of galaxies
123 with a narrow range of stellar masses ($M_* \sim 10^{10} M_\odot$) in

a range of environments. GAMA is highly spectroscopically complete (97 per cent; Driver et al. 2011), even in the densest regions. This is achieved by returning to each target area an average of 10 times, as described in Robotham et al. (2010). This enables accurate environment measurements including 5th nearest neighbour surface densities (e.g. Wijesinghe et al. 2012) and friends-of-friends group determination (Robotham et al. 2011).

We describe the selection of our sample in Section 2 and the observations in Section 3. In Section 4 we describe the method for measuring the emission line properties and then present the total star formation rates and H α surface brightness profiles of the sample in Sections 5 and 6. We discuss our findings in Section 7 before summarising our conclusions in Section 8. Throughout this paper we assume a Hubble constant of $H_0 = 70 \text{ km s}^{-1} \text{ Mpc}^{-1}$ and $\Omega_M = 0.3$, $\Omega_\Lambda = 0.7$. Equivalent widths for features in emission are quoted as positive numbers.

2 SAMPLE

We selected our sample from the Galaxy And Mass Assembly (GAMA; Driver et al. 2011¹) survey which combines single-fibre spectroscopy (Hopkins et al. 2013) with a diverse set of supporting imaging data. We specifically selected galaxies from the first phase of the GAMA survey, referred to as GAMA I. There are $\sim 170,000$ galaxies in the GAMA I sample down to $r = 19.4$ mag in two regions, each of 48 sq deg, and $r = 19.8$ mag in a third region, also of 48 sq deg. While the majority of the GAMA spectra have been obtained from the Anglo-Australian Telescope (AAT), the spectra and redshifts for brighter galaxies in these regions, like those targeted here, are obtained from the Sloan Digital Sky Survey (SDSS; York et al. 2000).

In order to focus specifically on the effects of environment rather than stellar mass we targeted galaxies with stellar masses $6 \times 10^9 M_\odot < M_* < 2 \times 10^{10} M_\odot$. The stellar mass measurements are from spectral energy distribution fits to optical broad-band photometry (Taylor et al. 2011) and have random uncertainties of ~ 0.3 dex. Given the size of the uncertainties, no narrower window in stellar mass would be appropriate. We corrected the redshifts for the effects of peculiar velocity using the Tonry et al. (2000) multi-attractor flow model (z_{TONRY} ; Baldry et al. 2012) and limited the sample to low redshifts, $0.02 < z_{\text{TONRY}} < 0.06$, so that targets are close enough that we can spatially resolve them. This reduces the available sample to 688 galaxies. We are complete in stellar mass over the redshift range considered.

The nearest neighbour surface density, Σ_5 , is calculated for all galaxies with reliable redshifts ($nQ > 2$; Driver et al. 2011). The 5th nearest neighbour metric is similar to the Σ_1 metric used in Brough et al. (2011). The surface density is defined using the projected co-moving distance to the 5th nearest neighbour (d_5) with $\pm 1000 \text{ km s}^{-1}$ within a pseudo-volume limited density-defining population: $\Sigma_5 = 5/\pi d_5^2$. The density-defining population has absolute SDSS petrosian magnitudes $M_r < M_{r,\text{limit}} - Qz$, k-corrected to $z = 0$ following Loveday et al. (2012), where $M_{r,\text{limit}} = -20.0$ mag

and Q defines the expected evolution of M_r as a function of redshift ($Q=0.87$; Loveday et al. 2012). Densities are then corrected for the survey r -band redshift completeness as $\Sigma_5 = \Sigma_{5,\text{raw}} \times 1/\text{completeness}$. Galaxies where the nearest survey edge is closer than the 5th nearest neighbour have upper limits calculated and flags assigned. More details on this and other environment metrics available for GAMA will be provided in Brough et al. (in prep).

There are 424 galaxies with stellar masses $6 \times 10^9 M_\odot < M_* < 2 \times 10^{10} M_\odot$ and $0.02 < z_{\text{TONRY}} < 0.06$ that are not flagged as having been affected by a survey edge. These 424 galaxies have environmental densities $0.02 < \Sigma_5 (\text{Mpc}^{-2}) < 78$, with a median $\Sigma_5 = 0.77 \text{ Mpc}^{-2}$. We randomly selected 18 galaxies across 2 density bins around the median density ($< 0.77 \text{ Mpc}^{-2}$; 11 galaxies and $> 0.77 \text{ Mpc}^{-2}$; 7 galaxies). The surface density distribution of the 424 possible targets and the 18 selected are illustrated in Figure 1. The 18 targets selected have apparent SDSS petrosian magnitudes $m_r < 17.6$ mag and a mean effective semi-major axis radius, from 2D Sersic surface brightness fits to re-processed SDSS r-band imaging (Kelvin et al. 2012), of $R_{e,r} = 3.4''$. The properties of the 18 observed galaxies from the GAMA survey are described in Table 1.

We determined the effect the number of the nearest neighbour used has on the sample selected and the results presented here. We also calculated $\Sigma_{N=10}$ for the parent sample considered here (galaxies with stellar masses $6 \times 10^9 M_\odot < M_* < 2 \times 10^{10} M_\odot$ and $0.02 < z_{\text{TONRY}} < 0.06$). The mean difference $\Sigma_{N=5} - \Sigma_{N=10} = 2.0 \text{ Mpc}^{-1} \pm 6.8 \text{ Mpc}^{-1}$. The median $\Sigma_{N=10} = 0.95 \text{ Mpc}^{-1}$, which does not move galaxies between the high and low density bins defined here. However, using $N=10$ a large fraction of this sample (12 out of 18) are affected by survey edges, we therefore present all of our results using $N=5$.

The GAMA groups catalogue (Robotham et al. 2011) is not volume limited so we cannot draw strong conclusions from the group properties of these galaxies. However, we do note that all galaxies in high-density environments are found in groups and that these generally have higher total dynamical masses ($7 \times 10^{12} M_\odot < M_{\text{dyn}} < 4 \times 10^{14} M_\odot$) than the 3/11 galaxies in low-density environments that are found in pairs and groups ($7 \times 10^{11} M_\odot < M_{\text{dyn}} < 7 \times 10^{12} M_\odot$). For information we also indicate in Table 1 whether the galaxies in groups are the central galaxy in their group (C), a satellite (S) or one of a pair of galaxies (P), where the group centre is defined following an iterative centre-of-light analysis (Robotham et al. 2011). None of these galaxies are at the centre of a group.

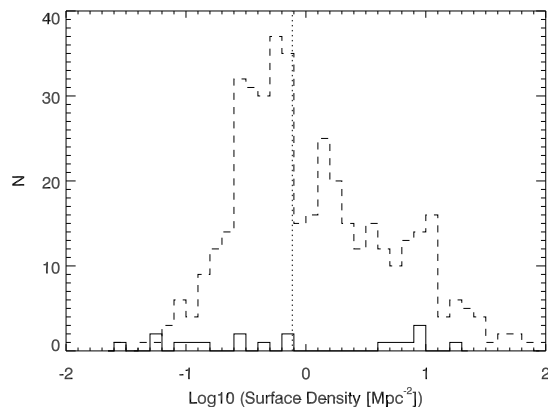
3 OBSERVATIONS

The data were taken in 2011 April, 2012 February and 2012 May with the SPIRAL IFU. SPIRAL is a 32×16 element rectangular microlens array coupled via an optical fibre feed to the dual-beam AAOmega spectrograph (Saunders et al. 2004; Sharp et al. 2006). It has a spatial sampling of $0''.7/\text{spaxel}$ with no gaps, giving a field of view of $22''.4 \times 11''.2$. We observed with the low-resolution 580V grating in the blue and the higher resolution 1000R grating in the red. These settings correspond to wavelength ranges of 3700–5700Å and 6200–7300Å and spectral resolutions of

¹ <http://www.gama-survey.org>

Table 1. Properties of the observed sample of galaxies from GAMA (described in the text). The galaxies are divided into the two environmental density bins: high density (top of table) and low density (bottom of table).

| GAMA ID | RA J2000 | Dec. J2000 | Stellar Mass Log(M_{\odot}) | z_{TONRY} | Σ_5 Mpc^{-2} | Group Mass Log(M_{\odot}) | Central? | $R_{e,r}$ " | Sersic n_r |
|---------|-------------|---------------|------------------------------------|--------------------|---------------------------------|----------------------------------|----------|----------------|--------------|
| 136624 | 11:43:17.06 | -01:38:39.0 | 10.30 | 0.0463 | 16.33 | 13.8 | S | 2.24 | 2.4 |
| 220328 | 12:04:16.65 | +01:32:46.5 | 9.83 | 0.0221 | 9.91 | 13.8 | S | 5.20 | 2.5 |
| 618152 | 14:18:05.49 | +00:13:38.6 | 10.03 | 0.0543 | 8.25 | 14.6 | S | 3.56 | 0.9 |
| 227278 | 14:11:19.16 | +01:18:34.3 | 10.13 | 0.0259 | 8.06 | 12.8 | S | 2.05 | 2.6 |
| 600916 | 09:12:06.92 | +00:20:12.7 | 10.05 | 0.0549 | 7.71 | 12.9 | S | 5.50 | 1.1 |
| 136880 | 11:45:20.90 | -01:48:46.1 | 9.78 | 0.028 | 6.04 | 13.8 | S | 3.79 | 1.6 |
| 600978 | 09:12:45.34 | +00:20:24.9 | 9.91 | 0.0549 | 4.89 | 12.9 | S | 5.08 | 0.8 |
| 422359 | 08:42:13.17 | +02:37:28.6 | 10.10 | 0.051 | 0.71 | - | | 2.47 | 1.6 |
| 106252 | 14:21:05.39 | +00:51:54.3 | 9.83 | 0.0550 | 0.65 | - | | 2.34 | 0.6 |
| 227962 | 14:22:01.09 | +01:11:50.3 | 9.88 | 0.0558 | 0.42 | 12.8 | S | 2.02 | 0.9 |
| 92770 | 14:30:14.98 | +00:37:17.0 | 9.87 | 0.0271 | 0.31 | - | | 3.28 | 1.2 |
| 418448 | 09:04:50.24 | +02:30:23.3 | 10.02 | 0.0557 | 0.26 | - | | 2.03 | 2.5 |
| 375909 | 08:45:32.05 | +01:17:36.0 | 9.96 | 0.0450 | 0.14 | 12.9 | P | 4.23 | 0.8 |
| 536005 | 12:00:00.48 | -01:01:40.7 | 10.09 | 0.0483 | 0.12 | - | | 2.62 | 1.4 |
| 535319 | 11:49:15.69 | -00:58:36.9 | 9.89 | 0.0606 | 0.09 | 11.9 | P | 4.08 | 0.8 |
| 55150 | 12:03:01.01 | -00:17:28.2 | 10.09 | 0.0417 | 0.06 | - | | 4.47 | 0.7 |
| 371177 | 08:41:39.24 | +00:58:26.7 | 10.03 | 0.0608 | 0.06 | - | | 2.63 | 1.7 |
| 583637 | 11:43:17.98 | -00:10:53.8 | 10.01 | 0.0577 | 0.03 | - | | 3.28 | 1.2 |

**Figure 1.** Histogram showing the surface density distributions of the 424 possible targets (dashed line) and the 18 observed galaxies (solid line). The dotted line indicates the median surface density of 0.77 Mpc^{-2} that divides the low and high density samples analysed here. The observed galaxies sample the possible density distribution well and the low and high-density subsamples can be seen to be well separated.

1900 and 5000 respectively. Accounting for the sample redshift range, this targets the emission lines $H\beta$ in the blue and $H\alpha$ in the red. Observations were made during dark time, with an average seeing of $1.5''$ (FWHM). Each galaxy was observed for 3×2400 s with individual observations dithered by 1-2 spaxels in Right Ascension and Declination in order to avoid four isolated dead elements in SPIRAL. Spectrophotometric standard stars were also observed each night, in order to prepare a sensitivity function.

Initial data reduction, from raw detector output to dark-subtracted, bias-subtracted, wavelength-calibrated, sky-subtracted, 1D-extracted spectra, was achieved using

the 2dfdr pipeline (Croom et al. 2004). The root mean square dispersion around the wavelength solution is 0.12\AA in the blue and 0.03\AA in the red spectra. The dispersion around the 5577\AA sky line is 0.09\AA . Twilight flat-field frames were also observed in order to account for relative fibre-to-fibre transmission variations. As none of our targets completely fill the SPIRAL field-of-view a sky background spectrum was calculated by taking the median over pixels without galaxy light. The final data analysis was carried out using custom IDL routines. The sensitivity function determined from comparing the total observed flux from spectrophotometric standard stars to that predicted as a function of wavelength was applied. The final flux calibration was done by applying SDSS g - and i -band fiber magnitudes (measured in the $3''$ SDSS fibre) to the blue and red SPIRAL spectra integrated over a $3''$ aperture respectively for each galaxy. The calculated offset was then applied to the individual SPIRAL spectra. Comparison with the flux-calibrated SDSS spectra indicates a 6 per cent uncertainty in the flux calibration level of the blue spectra (covering the $H\beta$ line) and 10 per cent in the red spectra (covering the $H\alpha$ line). Following flux calibration individual frames were aligned and mosaiced using telescope offset information. Frames are scaled based on a comparison of overlap regions in the mosaic, to account for minor variations in transparency and seeing.

4 EMISSION-LINE MEASURES

In order to examine the radial distribution of star formation, high signal-to-noise spectra were produced by combining spectra within annuli for each galaxy. Each annulus is defined as a radial de-projection of the galaxy, based on position angle and inclination information derived from GAMA analysis of SDSS imaging data (Kelvin et al. 2012). Prior to stacking, each spectrum from individual spaxels is velocity matched based on a velocity fields derived from emission and

285 absorption fits to a block-averaged (3x3 spaxel) data-cube.
 286 The [NII], H α , [NII] region is fitted with a four component
 287 model, three emission lines and H α absorption, assuming
 288 common velocities and widths for the emission components
 289 and with the ratio of the flux of the nitrogen lines fixed at
 290 3.28. The emission redshift is allowed to float with respect
 291 to that of the absorption line. Errors are estimated from a
 292 quadrature summation of the statistic values returned for
 293 the best-fit model and the parameter distribution from a
 294 bootstrap re-sampling of each composite spectrum.

295 Individual Gaussian fits to the H α and H β emission
 296 lines in each spaxel of each SPIRAL data-cube were also
 297 made for examination purposes. The resulting H α flux and
 298 velocity maps as well as SDSS thumbnail images for the same
 299 field-of-view are shown for each galaxy in Appendix A. The
 300 maps are presented in order of environmental density (high-
 301 est density environment first). There are some interesting
 302 features in the H α flux maps including off-centre (600978,
 303 92770, 371177) and clumpy emission (618152, 535319, 55150,
 304 583637). Gerssen et al. (2012) also observe clumpy emission
 305 in their VIMOS IFU observations of SDSS galaxies. Two of
 306 the off-centre and clumpy emission features are in galaxies
 307 in high-density environments (618152 and 600978; 29^{+20}_{-11} per
 308 cent), while the remaining 5 are in galaxies in the low-density
 309 environments (45^{+15}_{-13} per cent). We conclude that off-centre
 310 and clumpy H α emission does not significantly depend on
 311 environment in our data.

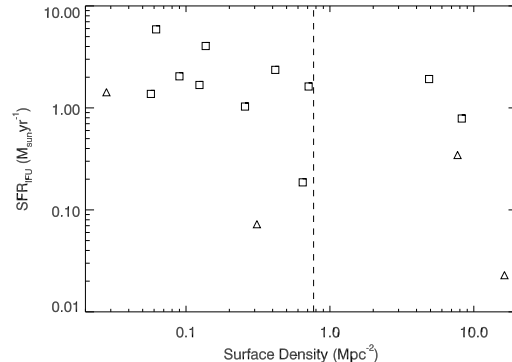
312 The H α velocity maps (Appendix A) show that all
 313 galaxies with strong H α emission show ordered rotation in
 314 that emission line, even when the emission is clumpy or off-
 315 centre. This is consistent with observations at higher red-
 316 shifts showing that clumpy galaxies are well fit by ordered
 317 disk models (e.g. Wisnioski et al. 2011).

318 5 STAR FORMATION RATES

319 We first examine the total star formation rates (SFR) of
 320 the galaxies. The total SFR measurements are made by
 321 summing the obscuration-corrected H α flux ($f_{H\alpha}$ [ergs s $^{-1}$
 322 cm $^{-2}$]) over the observed extent of the galaxy. The flux is
 323 obscuration corrected using the Balmer decrement (BD; H α
 324 flux/H β flux) measured in individual spaxels. The H α lu-
 325 minosity is then:

$$326 L_{H\alpha}(W) = 4\pi d_L^2 f_{H\alpha}(BD/2.86)^{2.36}, \quad (1)$$

327 where d_L is the luminosity distance in centimetres. The
 328 Balmer decrement is a unitless obscuration sensitive param-
 329 eter and its departure from the Case B recombination value
 330 of 2.86 indicates dust attenuation along the line of sight.
 331 While dust geometries are complex, this approach implic-
 332 itly models the dust as a foreground screen averaged over the
 333 galaxy (Calzetti 2001). The exponent in the dust obscura-
 334 tion correction factor is equal to $k(\lambda_{H\alpha})/[k(\lambda_{H\beta}) - k(\lambda_{H\alpha})]$,
 335 and $k(\lambda)$ at a given λ is determined from the Cardelli et al.
 336 (1989) Galactic dust extinction curve (derived from obser-
 337 vations of the UV extinction of stars). This is found to well
 338 describe the obscuration of the ionised gas in star-forming
 339 galaxies (Calzetti 2001; Gunawardhana et al. 2011). The
 340 SFRs are then calculated using the relationship given by
 341 Kennicutt (1998) assuming a Salpeter (1955) initial mass



342 **Figure 2.** Total star formation rates of the star-forming galaxies
 343 as a function of environmental density. The dashed line indicates
 the median surface density of 0.77 Mpc^{-2} that divides the low
 and high-density subsamples analysed here. There is a weak corre-
 344 lation between $\log_{10}(\text{SFR}_{\text{IFU}})$ and $\log_{10}(\Sigma_5)$, significant only at
 the 1.8σ level. We indicate which galaxies would have been clas-
 345 sified by Wijesinghe et al. (2012) as star forming (squares) and
 non-star forming (triangles); some of those classified as non-star
 346 forming are still forming stars.

347 function (IMF), i.e. $\text{SFR} = L_{H\alpha}(W)/1.27 \times 10^{34}$. These val-
 348 ues are given in Table 2.

349 5.1 Dependence on Environment

350 We compare the total SFRs of the star-forming galaxies
 351 (SFR_{IFU}) with their environmental density in the top panel
 352 of Figure 2. We note that the only absorption-dominated
 353 galaxy (galaxy 220328) in this sample is found in the high-
 354 est density environment. The observed mean SFR_{IFU} (low
 355 density) = 1.97 ± 0.51 is more than a factor of two higher
 356 than that at high density (= 0.77 ± 0.42). To determine
 357 the significance of an environmental dependence we apply
 a Kolmogorov-Smirnov two sample test to the SFRs in the
 low and high-density environments. This gives a probability
 of 19.6 per cent that the two samples are drawn from the
 same parent population. A Spearman rank correlation of the
 relationship between $\log_{10}(\Sigma_5)$ and $\log_{10}(\text{SFR})$, shows that
 the correlation between these parameters is only significant
 358 at the 1.8σ level.

359 Given the small size of our sample and the scatter ob-
 360 served we examine whether we can detect a significant rela-
 361 tionship with environment. We tested this by adjusting the
 362 mean SFRs of the galaxies in the high-density environments
 363 while maintaining their standard deviation and re-ran our
 364 statistical tests. A weakly significant correlation between en-
 365 vironment and SFR is observed (at a 2.3σ level) if the mean
 366 SFRs in high-density environments are a factor of 5 lower
 367 than those in the low-density environments (a factor of 2
 368 lower than observed).

369 We observe a weak but not significant relationship of
 370 SFR with environment in this sample. Due to the small
 371 sample size and observed scatter we cannot draw a strong
 372 conclusion about a universal SFR dependence, or lack of, on
 373 environment.

Table 2. Spectral measurements from IFU observations and the GAMA survey. Total H α fluxes and obscuration-corrected star formation rates (SFR) are given for the IFU observations. The GAMA measurements (described in the text) are made from SDSS stellar absorption-corrected single-fibre spectra. The column ‘Class’ details whether a galaxy is classified as an AGN by GAMA and whether it would be classified as Star Forming (SF) or Non-Star Forming (NSF) by Wijesinghe et al. (2012). The galaxies are divided into the two environmental density bins: high density (top of table) and low density (bottom of table). Galaxy 220328 only shows H α in absorption and Galaxies 136880 and 227278 are active galactic nuclei (AGN).

| GAMA ID | $f_{H\alpha,IFU}$ $10^{-17}\text{ergs s}^{-1}\text{ cm}^{-2}$ | SFR_{IFU} $M_{\odot}\text{yr}^{-1}$ | H β EW _{SDSS} \AA | BD _{GAMA} | SFR_{GAMA} $M_{\odot}\text{yr}^{-1}$ | Class |
|---------|--|---|--|--------------------|--|-------|
| 136624 | 266 | 0.02 | 0.10 | 1.50 | 0.01 | NSF |
| 220328 | - | - | -0.08 | 2.42 | 0.01 | NSF |
| 618152 | 618 | 0.79 | 4.21 | 4.57 | 1.58 | SF |
| 227278 | 85 | - | 0.66 | 3.37 | - | AGN |
| 600916 | 276 | 0.35 | 1.46 | 5.09 | 0.79 | NSF |
| 136880 | 44 | - | 0.10 | 5.22 | - | AGN |
| 600978 | 1608 | 1.92 | 6.92 | 3.96 | 2.14 | SF |
| 422359 | 1328 | 1.62 | 6.10 | 4.32 | 2.13 | SF |
| 106252 | 165 | 0.19 | 3.23 | 5.13 | 0.64 | SF |
| 227962 | 1930 | 2.36 | 8.38 | 3.61 | 1.87 | SF |
| 92770 | 366 | 0.07 | 0.69 | 3.07 | 0.04 | NSF |
| 418448 | 793 | 1.03 | 4.19 | 3.62 | 0.88 | SF |
| 375909 | 2976 | 4.04 | 8.43 | 4.85 | 5.09 | SF |
| 536005 | 2140 | 1.68 | 8.76 | 4.57 | 4.11 | SF |
| 535319 | 1425 | 2.04 | 6.42 | 3.75 | 1.72 | SF |
| 55150 | 5630 | 5.89 | 5.91 | 4.27 | 4.26 | SF |
| 371177 | 730 | 1.37 | 3.00 | 3.41 | 0.56 | SF |
| 583637 | 958 | 1.42 | 2.18 | 4.04 | 0.65 | NSF |

5.2 Comparison with Wijesinghe et al. (2012)

We use the total SFR measurements made from our IFU observations to analyse the Wijesinghe et al. (2012) star-forming galaxy classification. They define star-forming galaxies as those not classified as active galactic nuclei (AGN) using the Kewley et al. (2001) definition with non-absorption corrected H β equivalent widths (EW) $> 1.5\text{\AA}$, BD < 15 and SFR $> 10^{-3}M_{\odot}\text{yr}^{-1}$. We use the single-fibre GAMA measurements to determine whether our sample would meet their star-forming classification.

GAMA utilises the MPA/JHU emission-line catalogue² to obtain absorption-corrected line fluxes and equivalent widths (EW) for these bright galaxies. These line measurements are made from stellar absorption-corrected SDSS spectra. The GAMA SFRs are calculated as described in Hopkins et al. (2013) and Gunawardhana et al. (2013) and are given in Table 2. In summary, the H α luminosity is calculated from the H α EW, which is aperture corrected and extinction corrected using the Balmer decrement as per the IFU measurements. The GAMA SFRs are then calculated using the Kennicutt (1998) relationship. We note that dust obscuration is not excessive in any of the galaxies in this sample: their mean Balmer decrements are 3.9 ± 0.9 (Table 2) which translates to a dust obscuration factor of ~ 2 .

Wijesinghe et al. (2012) do not correct H β equivalent widths for stellar absorption for the definition of their star-forming sample, however, they do correct H α equivalent widths by adding a constant correction of 0.7\AA . We therefore use that addition here, i.e. stellar absorption corrected H β EW $> 2.2\text{\AA}$, to determine whether our sample would meet

their star-forming classification. Table 2 shows that 2 of the galaxies in this sample are classified as AGN from the single-fibre analysis and 5 do not make the Wijesinghe et al. (2012) star-forming classification, based on their H β EW. Figure 2 shows that 4 of these ‘non-star forming’ galaxies are still forming stars at some level. These galaxies are a clear indication of the need to take care when separating galaxies into distinct star-forming and non-star-forming populations.

5.3 Aperture Corrections

Calculating the total SFR of galaxies from single-fibre observations requires a correction for the portion of the galaxy enclosed by the size of the fibre used: an aperture correction. In the GAMA survey the total SFR is calculated by aperture correcting the H α flux measured within the fibre following the method of Hopkins et al. (2003). This aperture correction relies on the assumption that the line emission scales directly with the stellar continuum, as measured by the r -band magnitude. However, there is obviously some uncertainty in that assumption. We use the total SFR measurements made from our IFU observations to analyse this correction further. The IFU SFR are compared to the GAMA SFR in the top panel of Figure 3.

We do not include either galaxy 220328 or the two AGN in this analysis due to a lack of observable star formation and AGN contamination respectively. The mean difference $\text{SFR}_{GAMA}/\text{SFR}_{IFU} = 1.26 \pm 0.23, \sigma = 0.90$ i.e. SFR_{GAMA} is on average 26 per cent higher than SFR_{IFU} with a broad dispersion (the standard error on the mean is calculated as σ/\sqrt{N}).

Gerssen et al. (2012) analysed the aperture correction applied to calculate total SFR from SDSS spectra by Brinch-

² <http://www.mpa-garching.mpg.de/SDSS/DR7/>

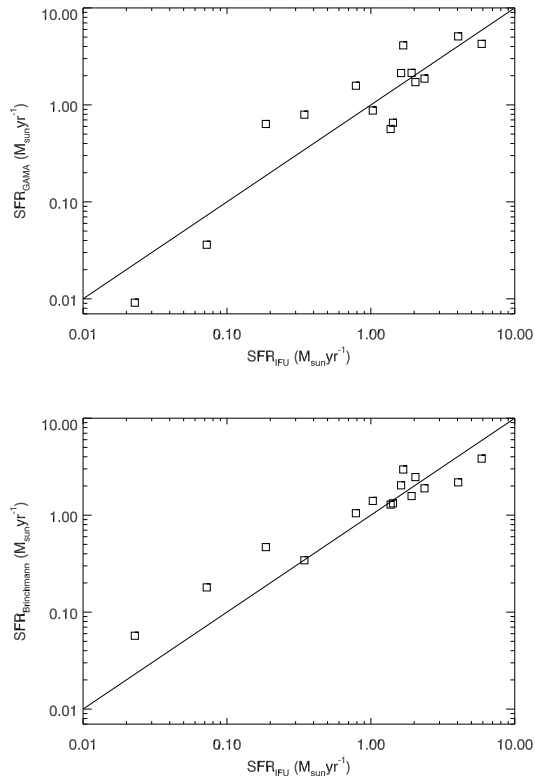


Figure 3. Comparing total star formation rates from IFU and single-fibre observations of the star-forming galaxies. The solid lines indicate the 1:1 relationships. The *top panel* shows the comparison between the total IFU star formation rates and the total aperture-corrected GAMA single-fibre star formation rates. The mean ratio is $\text{SFR}_{\text{GAMA}}/\text{SFR}_{\text{IFU}} = 1.26 \pm 0.23$. The *lower panel* shows the comparison between the total IFU star formation rates and the total SDSS single-fibre SFR aperture-corrected as per Brinchmann et al. (2004). The mean ratio $\text{SFR}_{\text{Brinchmann}}/\text{SFR}_{\text{IFU}} = 1.34 \pm 0.17$. The aperture-corrected SFRs are in relatively good agreement with those from the IFU measurements, no matter which aperture correction method is used. However, the uncertainties can still be large for individual systems.

mann et al. (2004) using IFU observations of 24 star-forming ($H\alpha\text{EW} > 20\text{\AA}$, $f_{H\alpha} > 448 \times 10^{-17} \text{ ergs s}^{-1} \text{ cm}^{-2}$), low-mass ($1 \times 10^8 M_{\odot} < M_{*} < 3 \times 10^{10} M_{\odot}$) SDSS galaxies. They found the Brinchmann et al. (2004) aperture corrections to underestimate the total SFR by a factor of 2.5 with a dispersion of 1.75, significantly larger than the factor of 1.26 difference and 0.90 dispersion we find between our IFU SFR and the GAMA aperture-corrected SFRs. We analyse whether the GAMA aperture correction is significantly different to that used by Brinchmann et al. (2004) by also comparing SFR_{IFU} with the most recent total SFR estimated by Brinchmann for the SDSS DR7 data release³ in the bottom panel of Figure 3.

Brinchmann et al. (2004) determine total SFRs using a Bayesian approach to calculate the likelihood of fits of the

observed spectrum to Charlot & Longhetti (2001) models, which incorporate an obscuration model. They note that, to first approximation, the dust corrections are based on the $H\alpha/H\beta$ ratio. The Brinchmann et al. (2004) total SFR are calculated with a Kroupa (2001) IMF and we convert to the Salpeter (1955) IMF used here by multiplying their measurements by 1.5. They aperture correct in an empirical manner using the distribution of the SFR/M^{*} ratio at a given $(g-r, r-i)$ colour and the photometry outside the fibre to correct the fibre SFR. This aperture correction is updated for the DR7 data release by calculating the light outside the fibre for each galaxy, and then fitting stochastic models to the photometry.

We find a mean difference $\text{SFR}_{\text{Brinchmann}}/\text{SFR}_{\text{IFU}} = 1.34 \pm 0.17$, $\sigma = 0.67$, i.e. we also find that the Brinchmann correction overestimates the SFR. This is a much smaller difference than Gerssen et al. (2012) found. This also suggests a marginal trend toward higher SFR estimates by aperture correcting using either method, although again with a high dispersion. These results suggest that contrary to the claim by Gerssen et al. (2012), the aperture-corrected SFRs for these low-mass galaxies are in relatively good agreement with those estimated from the IFU measurements, no matter which method is used. The large dispersion does however mean that the uncertainties can still be large for individual systems. In addition, this is still only a small sample, and reliable statistics on total SFR estimates compared to those from aperture-corrected measurements will need a much larger sample.

6 RADIAL $H\alpha$ PROFILES

We determine whether any dependence of SFR on environment is evident in the spatial distributions of $H\alpha$ emission in these galaxies.

The $H\alpha$ surface brightness is calculated by dividing the summed flux in each elliptical annulus by the area of the annulus. These radial profiles are shown in Figure 4.

Figure 4 shows that the radial $H\alpha$ surface brightness profiles of galaxies in both environments (solid and dashed lines) are very similar to one another, being centrally concentrated with high surface brightnesses over all radii studied. In contrast, the surface brightness profiles of the galaxies with no emission above the detection limit of $2 \times 10^{18} \text{ ergs s}^{-1} \text{ cm}^{-2} \text{ arcsec}^{-2}$ (dotted lines) are only present in the highest density environments. Of these, galaxy 220328 is dominated by absorption and the 2 AGN (136880, 227278) show central emission (dot-dashed lines) and no significant emission beyond that.

We further analyse the relationship of the profiles of the star-forming galaxies with their environment with straight-line fits to the $H\alpha$ surface brightness profiles taking into account the uncertainties in the $H\alpha$ flux measurements. We do not include the 3 galaxies with undetected emission in this analysis. We show the fitted gradient and intercept values and 1σ errors of the 15 star-forming galaxies as a function of environment in Figure 5.

We test the correspondence between these parameters with a Spearman rank correlation, finding that the gradients are correlated with $\log_{10}(\Sigma_5)$ at a significance of only 0.25σ and the intercepts are correlated at a significance of 0.4σ .

³ These are the total values given in gal_totsfr_dr7_v5.2.fits available at: <http://www.mpa-garching.mpg.de/SDSS/DR7/sfrs.html>

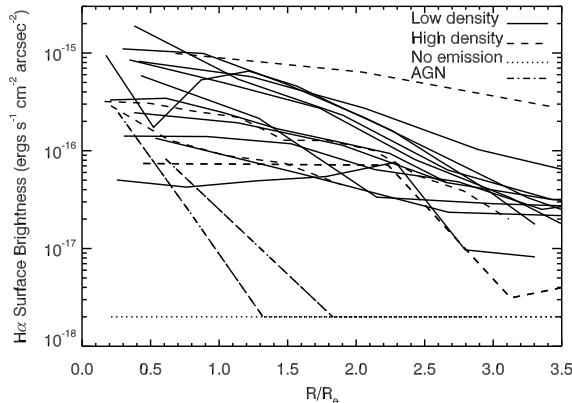


Figure 4. Radial H α surface brightness profiles as a function of the effective radius of the galaxy. Solid lines show galaxies in low-density environments ($< 0.77 \text{ Mpc}^{-2}$) and dashed lines show galaxies in high-density environments ($> 0.77 \text{ Mpc}^{-2}$), dotted lines indicate regions that do not show emission above the detection limit of $2 \times 10^{18} \text{ ergs s}^{-1} \text{ cm}^{-2} \text{ arcsec}^{-2}$ and dot-dashed lines indicate the emission of the two AGN. The average seeing approximates to $R/R_e \sim 0.2$. The profiles do not show a dependence on environment.

510 There is no dependence of the radial distribution of the H α
511 emission as a function of environment.

512 The galaxies observed here all have very similar stellar
513 masses and we are observing no significant dependence in
514 either H α surface brightness profile shape or amplitude of
515 the star-forming galaxies as a function of environment.

516 7 DISCUSSION

517 We have presented observations of the spatially-resolved H α
518 emission of galaxies over a wide range of environment with
519 the aim of examining how the radial distribution of star forma-
520 tion varies as a function of environment. We observe a
521 weak but not significant difference in total star formation
522 rate and no difference of radial profile of the star-forming
523 galaxies' H α emission as a function of local galaxy envi-
524 ronment in this sample of 18 galaxies with stellar masses
525 $\sim 10^{10} M_\odot$.

526 Before making general comments on the effect of envi-
527 ronment on star formation based on our observations,
528 we show that our sample is unbiased and representative of
529 the broader galaxy population in this narrow stellar mass
530 range. The uncertainties given below are 1σ binomial errors
531 (Cameron 2011). There are 424 galaxies in GAMA with ac-
532 curate surface densities (i.e. not affected by survey edges)
533 that have stellar masses, $6 \times 10^9 M_\odot < M_* < 2 \times 10^{10} M_\odot$,
534 and redshifts, $0.02 < z_{\text{TONRY}} < 0.06$. We use an updated
535 version of the Wijesinghe et al. (2012) classification (those
536 not classified as AGN with stellar absorption-corrected H β
537 $\text{EW} > 1.0 \text{ \AA}$, $\text{BD} < 15$ and $\text{SFR} > 10^{-3} M_\odot \text{ yr}^{-1}$) to quan-
538 tify star-forming galaxies. Of the 424 galaxies, there are
539 roughly equal numbers of AGN in each environmental den-
540 sity: 21/212 (10^{+2}_{-2} per cent) in low-density environments and
541 19/212 (9^{+2}_{-2} per cent) in high-density environments. There

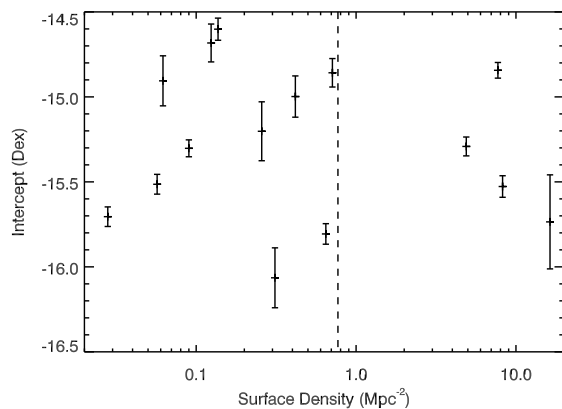
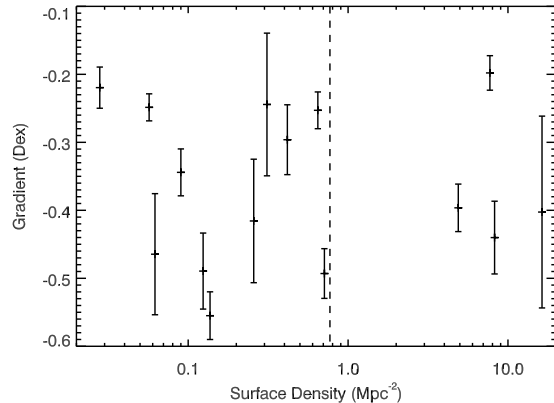


Figure 5. Parameters of straight-line fits to H α surface brightness profiles of the star-forming galaxies as a function of environmental density. The *top panel* shows the gradient of the fits. The gradients are correlated with environment at a significance of only 0.25σ . The *lower panel* shows the fitted intercept. The intercepts are correlated with environment at a significance of 0.4σ . The error bars show the 1σ uncertainties on the profile fits. The fits to the surface brightness profiles do not show a dependence on environment.

are 147/212 (69^{+3}_{-3} per cent) of galaxies in low-density environments that would make our star-forming galaxy criteria and 93/212 (44^{+3}_{-3} per cent) in high-density environments.

In the sample observed here, in the low-density environments, there are no AGN and 11/11 (100_{-14} per cent) of the galaxies make the updated star-forming galaxy criteria. In the high-density environment there are 2/7 (29^{+20}_{-11} per cent) AGN and a further 2/7 non-star-forming galaxies, meaning that 3/7 (43^{+18}_{-15} per cent) make our updated star-forming galaxy criteria.

We can conclude from this that the numbers of galaxies in this sample meeting the star-forming criteria in each environment are within 2.2σ of those in the broader sample. This sample therefore follows the distributions of the general population.

The sample studied here is broadly representative of the general population and we find that the total SFRs of the star-forming galaxies do not depend significantly on their local environmental density (Figure 2). However, due to the small size of the sample and the scatter observed we do not

draw a definitive conclusion about a possible SFR dependence on environment. Examining the spatial information provided by the H α surface brightness profiles, we observe no difference in amplitude or shape of the H α surface brightness profile of star-forming galaxies as a function of environment (Figures 4 and 5). We also find no evidence for ‘clumpiness’ in H α emission depending on environment (Appendix A).

The only comparable analysis to date examined the spatial star formation histories inferred from the colours of 44,964 galaxies in SDSS (Welikala et al. 2008). They found that the mean star formation rate of each galaxy as a function of radius is dominated by star formation in the central regions of galaxies, and that the trend for suppression in high-density environments is driven by a reduction in that central star formation. They also find that the mean star formation rate in the outskirts is independent of environmental effects. Welikala et al. (2008) conclude that the environment itself cannot suppress the star formation as the outer regions should otherwise be most affected and therefore this points to an evolutionary or AGN feedback origin. We do not observe any significant radial dependence of the surface brightness of H α emission as a function of environment, either centrally or in the outer regions. However, the suppression observed by Welikala et al. (2008) in their highest star-forming galaxies ($\text{SFR} > 1.02 M_{\odot} \text{yr}^{-1}$) is a factor of < 2 , of the order $\text{SFR} \sim 0.002 M_{\odot} \text{yr}^{-1}$. This difference is significantly smaller than we can detect with these observations so we cannot rule out the suppression they observe. Welikala et al. (2009) considered the density-morphology relation in the same sample, observing the strongest relation in the lowest luminosity galaxies with the highest star formation rates. However, they conclude that it cannot solely explain the observed suppression of star formation in galaxies in high-density environments. Table 1 shows that 3 out of the 4 galaxies with Sersic $n_r > 2$ are in high-density environments, of which 2 are not star forming. The mean n (high density) = 1.7 ± 0.3 and (low density) = 1.2 ± 0.2 , suggesting that there are signs of a difference in morphology as a function of environment in our sample but that it alone does not explain the lack of significant dependence of star formation on environment.

If these observations are borne out in larger samples, then combined with the known decreasing fraction of star-forming galaxies as a function of increasing environmental density (e.g. Balogh et al. 2004; Baldry et al. 2006; Bolzonella et al. 2010; McGee et al. 2011; Wetzel et al. 2012; Wijesinghe et al. 2012) and the small numbers of galaxies in transition between star forming and non-star forming observed in large samples (e.g. Wijesinghe et al. 2012; Mendel et al. 2013), this would suggest that if environment does drive the change in fractional contribution it must either act very rapidly (the ‘infall-and-quench’ model; e.g. Balogh et al. 2004; Bamford et al. 2008; Nichols & Bland-Hawthorn 2011; Wetzel et al. 2013) or have occurred a long time ago due to density-dependent evolution (an ‘in-situ evolution’ model; Wijesinghe et al. 2012), such that galaxies in transition are rare at this time. In-situ evolution would involve galaxies in dense environments evolving faster than galaxies in low-density environments, building their stellar mass faster and earlier, leading to the observed morphology-density relation, and consistent with the measured SFR-density relations at both low and high redshift. The in-situ evolution model is

similar to ‘downsizing’ (Cowie et al. 1996), ‘staged evolution’ (Noeske et al. 2007) and the ‘mass quenching’ model of Peng et al. (2010), however, galaxies of common mass would evolve differently in different environments in order to give rise to the observed population mix. Transition redshifts, at which the dependence of the specific star formation rates of galaxies on increasing environmental density transitions from increasing to decreasing, have been observed (e.g. Elbaz et al. 2007; Greene et al. 2012) giving weight to this argument.

We note that there are some caveats to this argument. Firstly, this is a small sample. A larger sample would increase the robustness of our results. Our sample also does not reach the densest cluster environments where galaxies are observed to be affected by ram pressure stripping (Owers et al. 2012; Merluzzi et al. 2013) and tidal distortions (e.g. Moss & Whittle 1993; Vogt et al. 2004; Bretherton et al. 2013). Our choice of environmental metric may play a role as the SFRs of galaxies at a fixed stellar mass have been observed to increase as a function of increasing cluster-centric radius, rather than environmental density (von der Linden et al. 2010; Rasmussen et al. 2012; Haines et al. 2013). In addition, van den Bosch et al. (2008) argue that the relationship between SFR and environment is driven by evolutionary differences between central and satellite galaxies in a dark-matter halo and we are only studying satellite galaxies here. We will examine the effects of our choice of environmental metric in a forthcoming paper (Brough et al., in prep.). Dust may also play a role as Koyama et al. (2013) find dustier galaxies in higher-density environments mask a trend of increasing specific SFR with increasing environmental density.

To separate the two scenarios of ‘infall-and-quench’ and ‘in-situ evolution’ and address these caveats requires observations of a very large sample of galaxies, covering a broad range of stellar mass and environment, in order to place stringent limits on the number density of any transition galaxies. It will be crucial to detect the very faintest levels of star formation present, as well as its spatial dependence. This will require very high signal-to-noise IFU spectra to enable careful decomposition of emission and absorption contributions (Sarzi et al. 2006). The new Sydney Australian Astronomical Observatory (AAO) Multi-object-IFU (SAMI; Croom et al. 2012) instrument with 13 deployable IFUs over a 1 degree field-of-view, and associated survey will enable this crucial next step.

8 CONCLUSIONS

We present observations of the spatially-resolved star formation as a function of local environment from optical integral field unit (IFU) observations of 18 galaxies with stellar masses $M_{*} \sim 10^{10} M_{\odot}$ selected from the GAMA survey. Our conclusions can be summarised as:

- The total star formation rates measured from the IFU data are consistent with the total aperture-corrected star formation rates measured from both the GAMA and SDSS surveys. The mean differences are $\text{SFR}_{\text{GAMA}}/\text{SFR}_{\text{IFU}} = 1.26 \pm 0.23$, $\sigma = 0.90$; $\text{SFR}_{\text{Brinchmann}}/\text{SFR}_{\text{IFU}} = 1.34 \pm 0.17$, $\sigma = 0.67$.

• Off-centre and clumpy H α emission does not depend on environment. It is present in 2/7 (29_{-11}^{+20} per cent) galaxies in high-density environments and 5/11 (45_{-13}^{+15} per cent) galaxies in low-density environments show similar features.

• In this sample, we see weak but not significant evidence of a dependence of total star formation rate on environment, using IFU observations for the first time.

• We observe no clear environmental trend on the amplitude or shape of the radial profile of H α emission. This implies that, for this sample, there is no strong outside-in or inside-out quenching.

• The lack of dependence of the radial profile of H α emission shape or amplitude on environment suggests that if environment drives the known change in fractional contribution of star-forming galaxies in different environments, it must either act very rapidly (the ‘infall-and-quench’ model) or galaxies must evolve in a density-dependent manner (an ‘in-situ evolution’ model), to explain the lack of transition galaxies observed in large samples.

In order to identify more precisely how and when any transition due to environment occurs requires high signal-to-noise, spatially-resolved spectra as well as a very large sample that covers a range in stellar mass, environment and star formation stage, including post-starburst galaxies. The new Sydney Australian Astronomical Observatory (AAO) Multi-object-IFU (SAMi; Croom et al. 2012) instrument will address this with its associated survey.

ACKNOWLEDGMENTS

We thank the anonymous referee for their comments which greatly improved the paper. SMC acknowledges the support of the Australian Research Council via a Future Fellowship (FT100100457). GAMA is a joint European-Australasian project based around a spectroscopic campaign using the Anglo-Australian Telescope. The GAMA input catalogue is based on data taken from the Sloan Digital Sky Survey and the UKIRT Infrared Deep Sky Survey. Complementary imaging of the GAMA regions is being obtained by a number of independent survey programs including GALEX MIS, VST KIDS, VISTA VIKING, WISE, Herschel-ATLAS, GMRT and ASKAP providing UV to radio coverage. GAMA is funded by the STFC (UK), the ARC (Australia), the AAO, and the participating institutions. The GAMA website is <http://www.gama-survey.org>.

REFERENCES

Baldry I. K., Balogh M. L., Bower R. G., Glazebrook K., Nichol R. C., Bamford S. P., Budavari T., 2006, *Monthly Notices of the RAS*, 373, 469

Baldry I. K., Driver S. P., Loveday J., Taylor E. N., Kelvin L. S., Liske J., Norberg P., Robotham A. S. G., et al., 2012, *Monthly Notices of the RAS*, 421, 621

Baldry I. K., Glazebrook K., Driver S. P., 2008, *Monthly Notices of the RAS*, 388, 945

Balogh M. L., Baldry I. K., Nichol R., Miller C., Bower R., Glazebrook K., 2004, *Astrophysical Journal, Letters*, 615, L101

Bamford S. P., Rojas A. L., Nichol R. C., Miller C. J., Wasserman L., Genovese C. R., Freeman P. E., 2008, *Monthly Notices of the RAS*, 391, 607

Bekki K., 2009, *Monthly Notices of the RAS*, 399, 2221

Blanton M. R., Lupton R. H., Schlegel D. J., Strauss M. A., Brinkmann J., Fukugita M., Loveday J., 2005, *Astrophysical Journal*, 631, 208

Bolzonella M., Kovač K., Pozzetti L., Zucca E., Cucciati O., Lilly S. J., Peng Y., Iovino A., et al., 2010, *Astronomy & Astrophysics*, 524, A76

Bretherton C. F., Moss C., James P. A., 2013, *Astronomy & Astrophysics*, 553, A67

Brinchmann J., Charlot S., White S. D. M., Tremonti C., Kauffmann G., Heckman T., Brinkmann J., 2004, *Monthly Notices of the RAS*, 351, 1151

Brough S., Hopkins A. M., Sharp R. G., Gunawardhana M., Wijesinghe D., Robotham A. S. G., Driver S. P., Baldry I. K., et al., 2011, *Monthly Notices of the RAS*, 413, 1236

Calzetti D., 2001, *Publications of the Astronomical Society of the Pacific*, 113, 1449

Cameron E., 2011, *Publications of the Astronomical Society of Australia*, 28, 128

Cardelli J. A., Clayton G. C., Mathis J. S., 1989, *Astrophysical Journal*, 345, 245

Charlot S., Longhetti M., 2001, *Monthly Notices of the RAS*, 323, 887

Cluver M. E., Appleton P. N., Ogle P., Jarrett T. H., Rasmussen J., Lisenfeld U., Guillard P., Verdes-Montenegro L., et al., 2013, *Astrophysical Journal*, 765, 93

Cooper M. C., Newman J. A., Weiner B. J., Yan R., Willmer C. N. A., Bundy K., Coil A. L., Conselice C. J., et al., 2008, *Monthly Notices of the RAS*, 383, 1058

Cowie L. L., Songaila A., Hu E. M., Cohen J. G., 1996, *Astronomical Journal*, 112, 839

Croom S., Saunders W., Heald R., 2004, *Anglo-Australian Observatory Epping Newsletter*, 106, 12

Croom S. M., Lawrence J. S., Bland-Hawthorn J., Bryant J. J., Fogarty L., Richards S., Goodwin M., Farrell T., et al., 2012, *Monthly Notices of the RAS*, 421, 872

Driver S. P., Hill D. T., Kelvin L. S., Robotham A. S. G., Liske J., Norberg P., Baldry I. K., Bamford S. P., et al., 2011, *Monthly Notices of the RAS*, 413, 971

Elbaz D., Daddi E., Le Borgne D., Dickinson M., Alexander D. M., Chary R.-R., Starck J.-L., Brandt W. N., et al., 2007, *Astronomy & Astrophysics*, 468, 33

Ellison S. L., Patton D. R., Simard L., McConnachie A. W., 2008, *Astronomical Journal*, 135, 1877

Fumagalli M., Gavazzi G., 2008, *Astronomy & Astrophysics*, 490, 571

Gerssen J., Wilman D. J., Christensen L., 2012, *Monthly Notices of the RAS*, 420, 197

Gómez P. L., Nichol R. C., Miller C. J., Balogh M. L., Goto T., Zabludoff A. I., Romer A. K., Bernardi M., et al., 2003, *Astrophysical Journal*, 584, 210

Greene C. R., Gilbank D. G., Balogh M. L., Glazebrook K., Bower R. G., Baldry I. K., Hau G. K. T., Li I. H., McCarthy P., 2012, *Monthly Notices of the RAS*, 425, 1738

Gunawardhana M. L. P., Hopkins A. M., Bland-Hawthorn J., Brough S., Sharp R., Loveday J., Taylor E., Jones D. H., et al., 2013, *ArXiv e-prints*

Gunawardhana M. L. P., Hopkins A. M., Sharp R. G.,

- 799 Brough S., Taylor E., Bland-Hawthorn J., Maraston C., 861
800 Tuffs R. J., et al., 2011, Monthly Notices of the RAS, 415, 862
801 1647 863
- 802 Gunn J. E., Gott III J. R., 1972, Astrophysical Journal, 864
803 176, 1 865
- 804 Haines C. P., Pereira M. J., Smith G. P., Egami E., Sander- 866
805 son A. J. R., Babul A., Finoguenov A., Merluzzi P., et al., 867
806 2013, ArXiv e-prints 868
- 807 Hopkins A. M., Driver S. P., Brough S., Owers M. S., Bauer 869
808 A. E., Gunawardhana M. L. P., Cluver M. E., Colless M., 870
809 et al., 2013, Monthly Notices of the RAS, 430, 2047 871
- 810 Hopkins A. M., Miller C. J., Nichol R. C., Connolly A. J., 872
811 Bernardi M., Gómez P. L., Goto T., Tremonti C. A., et al., 873
812 2003, Astrophysical Journal, 599, 971 874
- 813 Hopkins P. F., Somerville R. S., Cox T. J., Hernquist L., 875
814 Jogee S., Kereš D., Ma C.-P., Robertson B., Stewart K., 876
815 2009, Monthly Notices of the RAS, 397, 802 877
- 816 Kapferer W., Sluka C., Schindler S., Ferrari C., Ziegler B., 878
817 2009, Astronomy & Astrophysics, 499, 87 879
- 818 Kauffmann G., White S. D. M., Heckman T. M., Ménard 880
819 B., Brinchmann J., Charlot S., Tremonti C., Brinkmann 881
820 J., 2004, Monthly Notices of the RAS, 353, 713 882
- 821 Kelvin L. S., Driver S. P., Robotham A. S. G., Hill 883
822 D. T., Alpaslan M., Baldry I. K., Bamford S. P., Bland- 884
823 Hawthorn J., et al., 2012, Monthly Notices of the RAS, 885
824 421, 1007 886
- 825 Kennicutt Jr. R. C., 1998, Annual Review of Astron and 887
826 Astrophys, 36, 189 888
- 827 Kewley L. J., Dopita M. A., Sutherland R. S., Heisler C. A., 889
828 Trevena J., 2001, Astrophysical Journal, 556, 121 890
- 829 Konstantopoulos I. S., Gallagher S. C., Fedotov K., Durrell 891
830 P. R., Heiderman A., Elmegreen D. M., Charlton J. C., 892
831 Hibbard J. E., et al., 2010, Astrophysical Journal, 723, 893
832 197 894
- 833 Koopmann R. A., Kenney J. D. P., 2004, Astrophysical 895
834 Journal, 613, 851 896
- 835 Koyama Y., Smail I., Kurk J., Geach J. E., Sobral D., 897
836 Kodama T., Nakata F., Swinbank A. M., et al., 2013, 898
837 Monthly Notices of the RAS 899
- 838 Kroupa P., 2001, Monthly Notices of the RAS, 322, 231 900
- 839 Larson R. B., Tinsley B. M., Caldwell C. N., 1980, Astro- 901
840 physical Journal, 237, 692 902
- 841 Lewis I., Balogh M., De Propriis R., Couch W., Bower R., 903
842 Offer A., Bland-Hawthorn J., Baldry I. K., Baugh C., 904
843 2002, Monthly Notices of the RAS, 334, 673 905
- 844 López-Sánchez Á. R., 2010, Astronomy & Astrophysics, 906
845 521, A63 907
- 846 López-Sánchez Á. R., Esteban C., Rodríguez M., 2004, As- 908
847 trophysical Journal, Supplement, 153, 243 909
- 848 López-Sánchez Á. R., Koribalski B. S., van Eymeren J., Es- 910
849 teban C., Kirby E., Jerjen H., Lonsdale N., 2012, Monthly 911
850 Notices of the RAS, 419, 1051 912
- 851 Loveday J., Norberg P., Baldry I. K., Driver S. P., Hopkins 913
852 A. M., Peacock J. A., Bamford S. P., Liske J., et al., 2012, 914
853 Monthly Notices of the RAS, 420, 1239 915
- 854 McCarthy I. G., Frenk C. S., Font A. S., Lacey C. G., 916
855 Bower R. G., Mitchell N. L., Balogh M. L., Theuns T., 917
856 2008, Monthly Notices of the RAS, 383, 593 918
- 857 McGee S. L., Balogh M. L., Wilman D. J., Bower R. G., 919
858 Mulchaey J. S., Parker L. C., Oemler A., 2011, Monthly 920
859 Notices of the RAS, 413, 996 921
- 860 Mendel J. T., Simard L., Ellison S. L., Patton D. R., 2013, 922
Monthly Notices of the RAS, 429, 2212
- Merluzzi P., Busarello G., Dopita M. A., Haines C. P.,
Steinhauser D., Mercurio A., Rifatto A., Smith R. J.,
Schindler S., 2013, Monthly Notices of the RAS, 429, 1747
- Meurer G. R., Hanish D. J., Ferguson H. C., Knezek P. M.,
Kilborn V. A., Putman M. E., Smith R. C., Koribalski B.,
et al., 2006, Astrophysical Journal, Supplement, 165, 307
- Moss C., Whittle M., 1993, Astrophysical Journal, Letters,
407, L17
- Nichols M., Bland-Hawthorn J., 2011, Astrophysical Jour-
nal, 732, 17
- Noeske K. G., Weiner B. J., Faber S. M., Papovich C., Koo
D. C., Somerville R. S., Bundy K., Conselice C. J., et al.,
2007, Astrophysical Journal, Letters, 660, L43
- Owers M. S., Couch W. J., Nulsen P. E. J., Randall S. W.,
2012, Astrophysical Journal, Letters, 750, L23
- Patton D. R., Torrey P., Ellison S. L., Mendel J. T., Scud-
der J. M., 2013, Monthly Notices of the RAS, 433, L59
- Peng Y.-j., Lilly S. J., Kovač K., Bolzonella M., Pozzetti
L., Renzini A., Zamorani G., Ilbert O., et al., 2010, As-
trophysical Journal, 721, 193
- Prescott M., Baldry I. K., James P. A., Bamford S. P.,
Bland-Hawthorn J., Brough S., Brown M. J. I., Cameron
E., et al., 2011, Monthly Notices of the RAS, 417, 1374
- Randall S., Nulsen P., Forman W. R., Jones C., Machacek
M., Murray S. S., Maughan B., 2008, Astrophysical Jour-
nal, 688, 208
- Rasmussen J., Mulchaey J. S., Bai L., Ponman T. J., Ray-
chaudhury S., Dariush A., 2012, Astrophysical Journal,
757, 122
- Rasmussen J., Ponman T. J., Verdes-Montenegro L., Yun
M. S., Borthakur S., 2008, Monthly Notices of the RAS,
388, 1245
- Robotham A., Driver S. P., Norberg P., Baldry I. K., Bam-
ford S. P., Hopkins A. M., Liske J., Loveday J., et al., 2010,
Publications of the Astronomical Society of Australia, 27,
76
- Robotham A. S. G., Liske J., Driver S. P., Sansom A. E.,
Baldry I. K., Bland-Hawthorn J., Brough S., et al., 2013,
Monthly Notices of the RAS, 416, 2640
- Robotham A. S. G., Norberg P., Driver S. P., Baldry I. K.,
Bamford S. P., Hopkins A. M., Liske J., Loveday J., et al.,
2011, Monthly Notices of the RAS, 416, 2640
- Rose J. A., Robertson P., Miner J., Levy L., 2010, Astro-
nomical Journal, 139, 765
- Salpeter E. E., 1955, Astrophysical Journal, 121, 161
- Sánchez S. F., Kennicutt R. C., Gil de Paz A., van de Ven
G., Vílchez J. M., Wisotzki L., Walcher C. J., Mast D.,
et al., 2012, Astronomy & Astrophysics, 538, A8
- Sarzi M., Falcón-Barroso J., Davies R. L., Bacon R., Bu-
reau M., Cappellari M., de Zeeuw P. T., Emsellem E.,
Fathi K., Krajnović D., Kuntschner H., McDermid R. M.,
Peletier R. F., 2006, Monthly Notices of the RAS, 366,
1151
- Saunders W., Cannon R., Sutherland W., 2004, Anglo-
Australian Observatory Epping Newsletter, 106, 16
- Scudder J. M., Ellison S. L., Mendel J. T., 2012, Monthly
Notices of the RAS, 423, 2690
- Sharp R., Saunders W., Smith G., Churilov V., Correll D.,
Dawson J., Farrel T., Frost G., et al., 2006, in Society
of Photo-Optical Instrumentation Engineers (SPIE) Con-
ference Series Vol. 6269 of Presented at the Society of

- 923 Photo-Optical Instrumentation Engineers (SPIE) Confer-
 924 ence, Performance of AAOmega: the AAT multi-purpose
 925 fiber-fed spectrograph
- 926 Smith R. J., Lucey J. R., Price J., Hudson M. J., Phillipps
 927 S., 2012, Monthly Notices of the RAS, 419, 3167
- 928 Strateva I., Ivezić Ž., Knapp G. R., Narayanan V. K.,
 929 Strauss M. A., Gunn J. E., Lupton R. H., Schlegel D.,
 930 et al., 2001, Astronomical Journal, 122, 1861
- 931 Strickland D. K., Heckman T. M., 2009, Astrophysical
 932 Journal, 697, 2030
- 933 Sun M., Donahue M., Voit G. M., 2007, Astrophysical Jour-
 934 nal, 671, 190
- 935 Taylor E. N., Hopkins A. M., Baldry I. K., Brown M. J. I.,
 936 Driver S. P., Kelvin L. S., Hill D. T., Robotham A. S. G.,
 937 et al., 2011, Monthly Notices of the RAS, 418, 1587
- 938 Thomas D., Maraston C., Schawinski K., Sarzi M., Silk J.,
 939 2010, Monthly Notices of the RAS, 404, 1775
- 940 Tonry J. L., Blakeslee J. P., Ajhar E. A., Dressler A., 2000,
 941 Astrophysical Journal, 530, 625
- 942 van den Bosch F. C., Aquino D., Yang X., Mo H. J.,
 943 Pasquali A., McIntosh D. H., Weinmann S. M., Kang X.,
 944 2008, Monthly Notices of the RAS, 387, 79
- 945 Veilleux S., Cecil G., Bland-Hawthorn J., 2005, Annual Re-
 946 view of Astron and Astrophys, 43, 769
- 947 Vogt N. P., Haynes M. P., Giovanelli R., Herter T., 2004,
 948 Astronomical Journal, 127, 3300
- 949 von der Linden A., Wild V., Kauffmann G., White S. D. M.,
 950 Weinmann S., 2010, Monthly Notices of the RAS, 404,
 951 1231
- 952 Welikala N., Connolly A. J., Hopkins A. M., Scranton R.,
 953 2009, Astrophysical Journal, 701, 994
- 954 Welikala N., Connolly A. J., Hopkins A. M., Scranton R.,
 955 Conti A., 2008, Astrophysical Journal, 677, 970
- 956 Wetzel A. R., Tinker J. L., Conroy C., 2012, Monthly No-
 957 tices of the RAS, 424, 232
- 958 Wetzel A. R., Tinker J. L., Conroy C., van den Bosch F. C.,
 959 2013, Monthly Notices of the RAS, 432, 336
- 960 Wijesinghe D. B., Hopkins A. M., Brough S., Taylor E. N.,
 961 Norberg P., Bauer A., Brown M. J. I., Cameron E., et al.,
 962 2012, Monthly Notices of the RAS, 423, 3679
- 963 Wisnioski E., Glazebrook K., Blake C., Wyder T., Martin
 964 C., Poole G. B., Sharp R., Couch W., et al., 2011, Monthly
 965 Notices of the RAS, 417, 2601
- 966 York D. G., Adelman J., Anderson Jr. J. E., Anderson
 967 S. F., Annis J., Bahcall N. A., Bakken J. A., Barkhouser
 968 R., et al., 2000, Astronomical Journal, 120, 1579

969 APPENDIX A: H α EMISSION-LINE MAPS

970 This paper has been typeset from a T \LaTeX / L \LaTeX file prepared
 971 by the author.

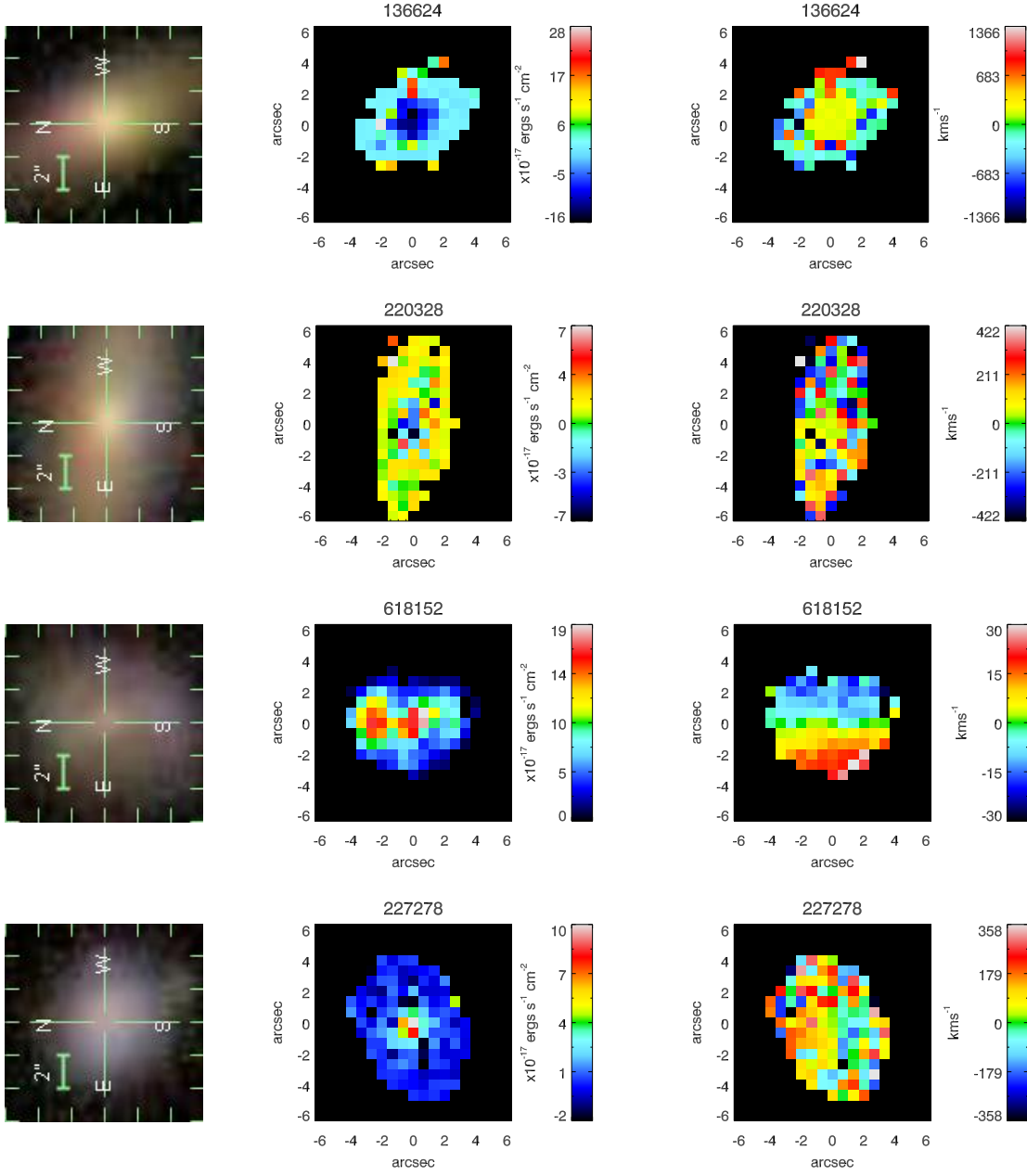


Figure A1. High-density environment galaxy sample. From left-to-right: SDSS thumbnail image of SPIRAL field-of-view, H α flux map of central region; H α velocity map of central region. Only spaxels with signal-to-noise ratios > 3 are shown.

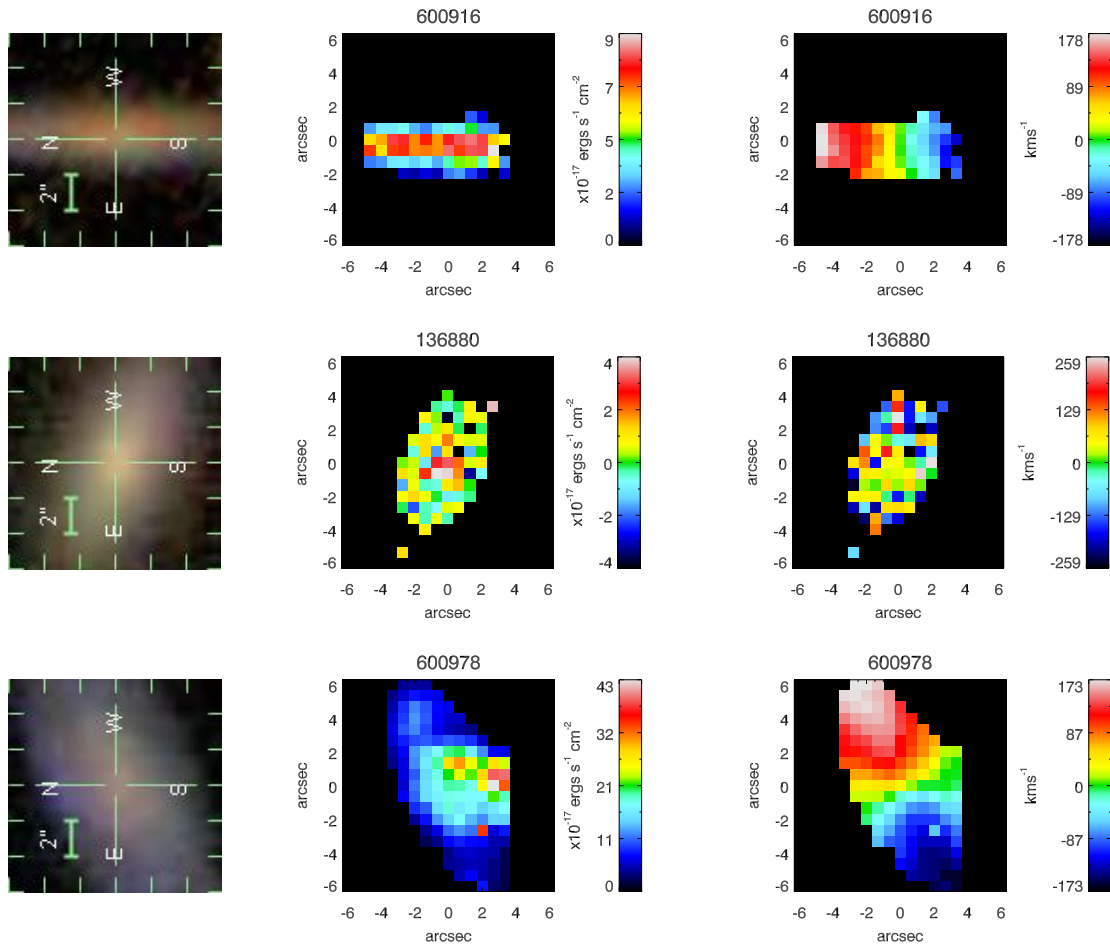


Figure A2. High-density environment galaxy sample - cont. From left-to-right: SDSS thumbnail image of SPIRAL field-of-view, H α flux map of central region; H α velocity map of central region. Only spaxels with signal-to-noise ratios > 3 are shown.

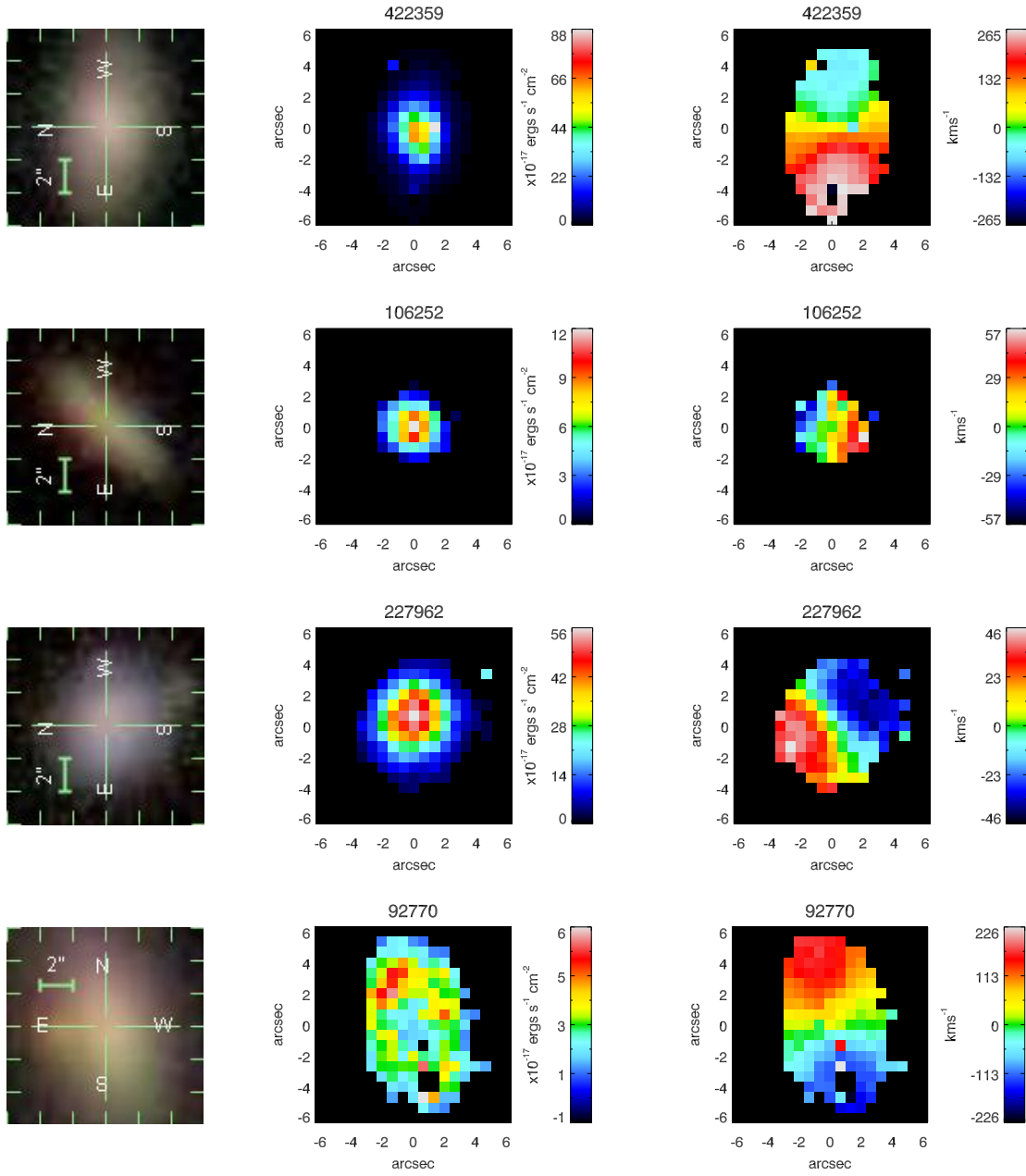


Figure A3. Low-density environment galaxy sample. From left-to-right: SDSS thumbnail image of SPIRAL field-of-view, H α flux map of central region; H α velocity map of central region. Only spaxels with signal-to-noise ratios > 3 are shown.

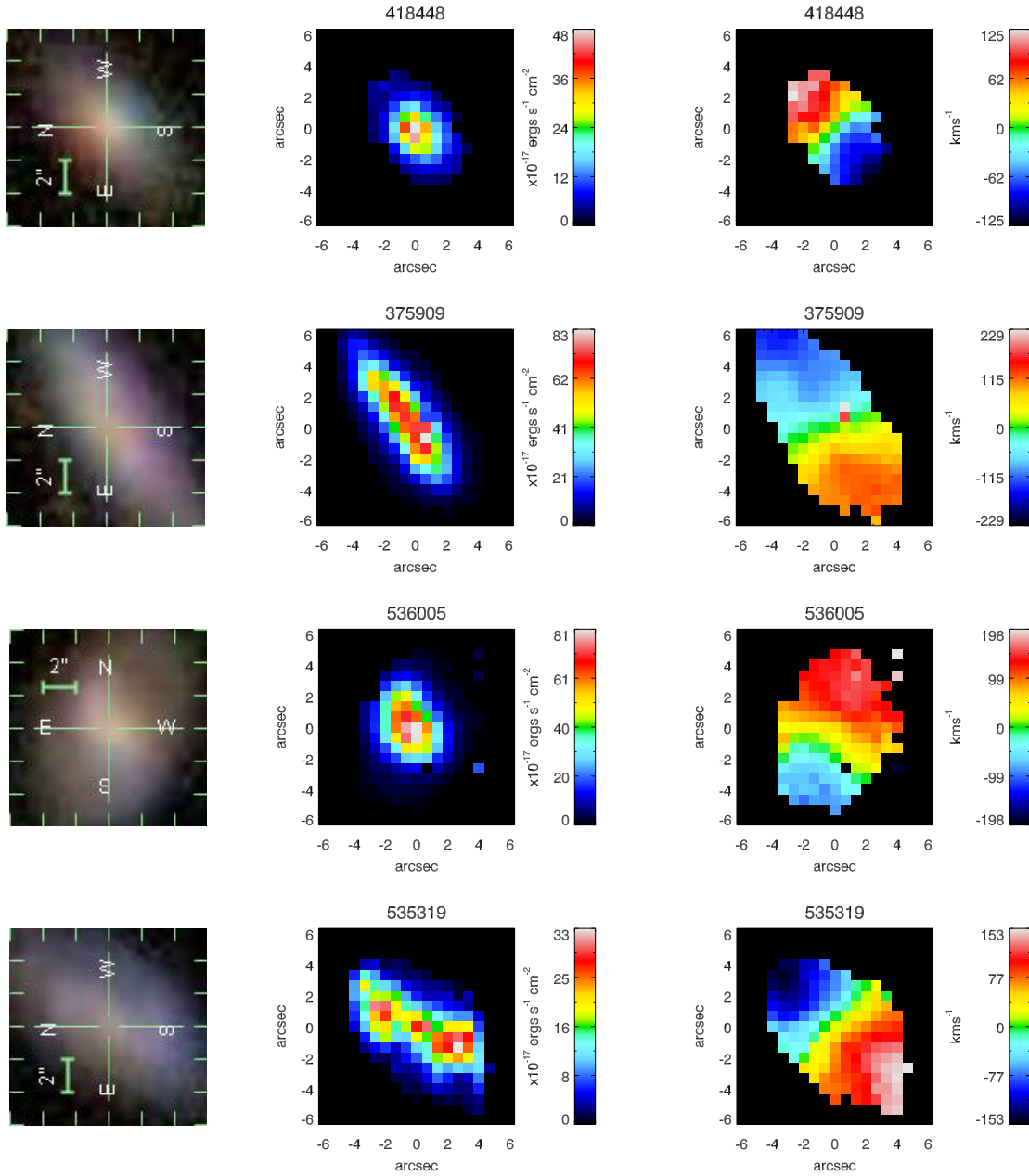


Figure A4. Low-density environment galaxy sample cont. From left-to-right: SDSS thumbnail image of SPIRAL field-of-view, H α flux map of central region; H α velocity map of central region. Only spaxels with signal-to-noise ratios > 3 are shown.

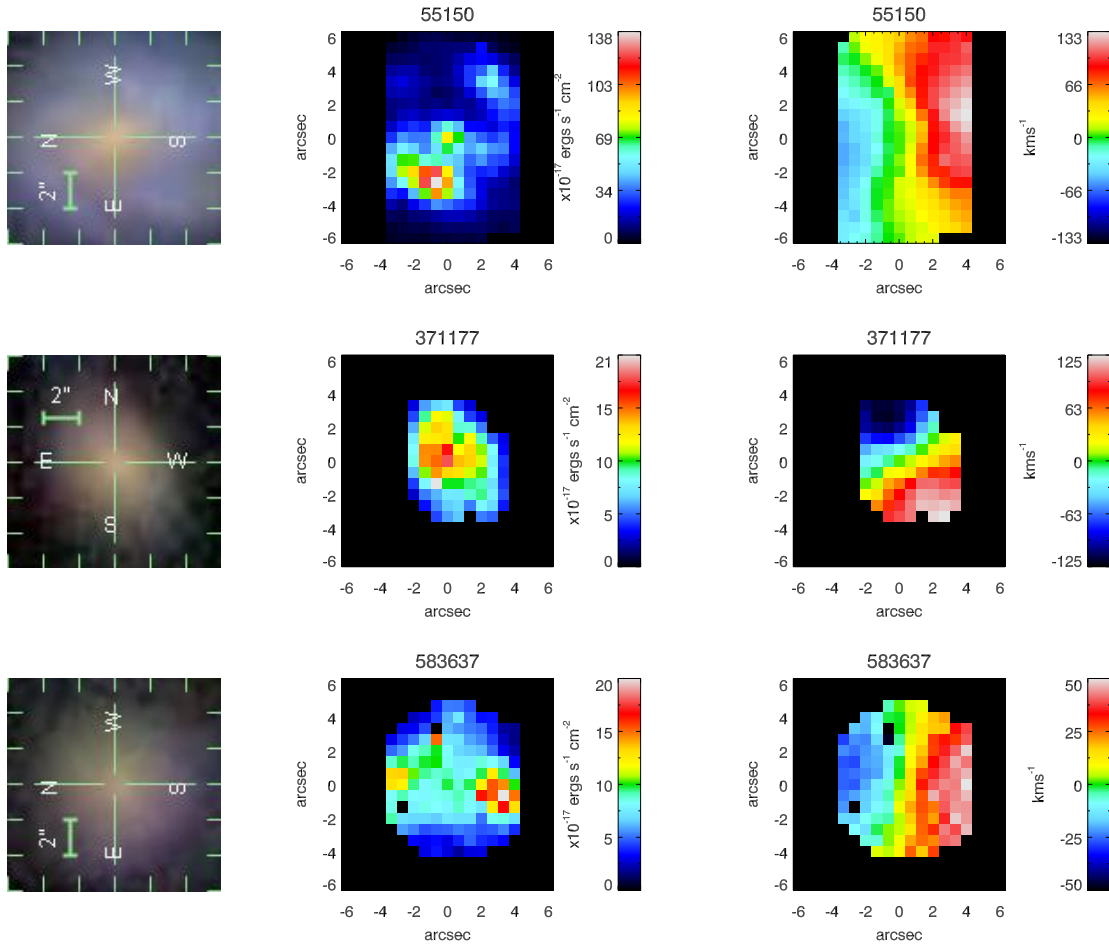


Figure A5. Low-density environment galaxy sample cont. From left-to-right: SDSS thumbnail image of SPIRAL field-of-view, H α flux map of central region; H α velocity map of central region. Only spaxels with signal-to-noise ratios > 3 are shown.